Microinclusions Impact on Steel Balls Fatigue Life

S. Rizzo[1], F. Morosi[1], R. Sesana[2], E. Ossola[2], E. Brusa[2]

[1] *Central Lab – Product Development, Tsubaki Nakashima, Italy*
[2] *DIMEAS, Politecnico di Torino, Italy*

Abstract – Rolling contact fatigue is the main cause of failure in bearings. Among other factors, damage phenomena are related to material properties and manufacturing processes. The damage evolution might be affected by microinclusions present in the material. This influence is related to composition, dimension, shape and location of microinclusions. The relation between microinclusions and fatigue life is investigated for balls undergoing Hertzian pressure fatigue for 100Cr6 steel. Failures are analysed to relate life of rolling elements to the microinclusion parameters.

Keywords – Bearing, Microinclusion, Rolling contact fatigue

1. Introduction

Bearing fatigue life is affected by several damage phenomena, including tribological conditions, surface and sub-surface defects and environmental conditions (temperature, corrosion and humidity) [1]. In optimal working conditions, the main cause of damage is Rolling Contact Fatigue (RCF) [2], which involves surface pitting and subsurface spalling. The main factor affecting sub-surface RCF damage is related to non-metallic inclusions, where the Hertzian contact shear stress is maximum [3]; in fact, inclusions act as stress risers, promoting crack initiation and propagation [4]. For this reason, steelmaking processes have improved steel cleanliness over the last decades [5,6], in order to control non-metallic inclusions (NMI) and oxides [7].

The effect of inclusions on fatigue life, considering the effect of size, shape, location and composition, is described in many studies [8–11]. In [12], experimental and numerical activities explored the stress state in the material around the inclusion, where microstructural changes were observed, referred as "butterfly wings".

Different inclusion sizes (ranging from 8 to 16 μm) were studied, but no strong influence on stress concentration was found. This result is partially in agreement with Gabelli et al. [13], who found that defects smaller than a threshold do not affect fatigue life of high strength steels for bearing manufacturing. In [14], basing on the Eshelby method, the interaction between multiple inclusions (pairs, clusters and stringers) was investigated. This paper presents an investigation on the effect of microinclusions on fatigue performance of a steel alloy (100Cr6) for rolling element manufacturing. This steel is defined in international Standards as UNI 3097 and DIN 17230 as 100Cr6, AISI/SAE as 52100, AFNOR 35-565 as 100C6. Many researches are dedicated to this steel, both with experimental and numerical approaches [7, 13, 15].

The purpose of the present paper is to correlate the bearing life and the incremented stress related to non-metallic inclusions presence in the subsurface of rolling balls during fatigue conditions. Microinclusions composition, shape, aspect ratio, geometry and location are obtained after the ball failure. An analytical model was implemented in a numerical dedicated solver, to relate life of rolling elements to the microinclusion parameters. A dedicated 3D model implementing Eshelby model [16] was developed to estimate the stress distribution around the microinclusion. This analysis introduces new contribution in the improvement of the quantitative estimation of bearing balls life. In particular the quantitative estimation of stress increment due to parameters related to microinclusion is included in life estimation. The estimations are then compared to actual failure cases.

2. Materials and methods

The fatigue performances of rolling elements have been evaluated by rig tests. Twelve cases of failures obtained under identical conditions were taken into account. Rig tests are structured with an electrical motor that drives a rotating shaft on which the inner rings of two double row ball bearings are trapped (figure 1) (inner ring curvature radii R2x = 22.250 mm and R2y = - 6.322mm). The rotary motion of the outer rings was prevented by the external fluted shell. The applied load was purely axial (34.4 kN) and it was guaranteed by a pneumo-hydraulic pistons system; tested bearings were assembled with 7 balls with diameter of 11.112 mm. The maximum pressure obtained on the ball surface from Hertz theory is of 3.8 GPa and the material is 100Cr6 steel. A correct lubrication status was guaranteed by the application of mineral grease. Once reached the ball failure, the evaluation of microinclusion effect on stresses was performed; the Eshelby-Mura model was applied to estimate the stress field surrounding each single microinclusion that was found in the spalling starting point. The stress modification due to a microinclusion is affected by its size, shape and location. Experimental evidence shows that inclusions can appear in pairs, clusters and stringers. The ASTM E45 Standard [17] provides a description for the stringer case, which is considered with a minimum of three particles. In this case, the stringer can be considered as a standalone inclusion with an elongated semi axis that covers the distance from the first to the

last inclusion. In addition, the stress peak at the inclusion boundary is affected by the depth at which the inclusion is located.

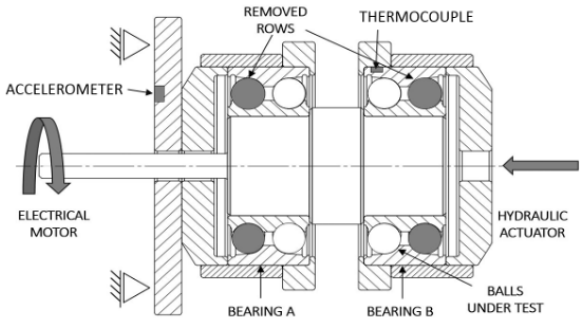

Figure 1: scheme of the test rig

3. Results and discussion

Twelve broken balls coming from the test were analized. In five cases, more than one inclusion was found in the fractured area; it was decided to consider only the one corresponding to the major increase of stress, since it was the worst from the fatigue life point of view. In addition, if inclusions with different chemical compositions were detected, a weighted average of Young's modulus and Poisson's ratio were used in the following calculations.

In figure 2, the nominal stress distribution obtained from the Hertz theory for a homogenous matrix is reported; and then for each single microinclusion, the corresponding calculated stresses were corrected taking into account for the composition, location and dimension of the inclusions experimentally found, by means of the Eshelby code. In particular a dedicated numerical solver was implemented in Matlab environment implementing the Eshelby equations to obtain the stress in the matrix volume around the microinclusion, given dimension, shape, material and position of the microdefect. Results are reported in Table 1. In the same table the calculation of the equivalent Tresca stresses [18] in uniform matrix σ_{nT} and at microinclusion boundaries with Eshelby's model σ_{iT} are reported for each microinclusion, accounting for dimension,

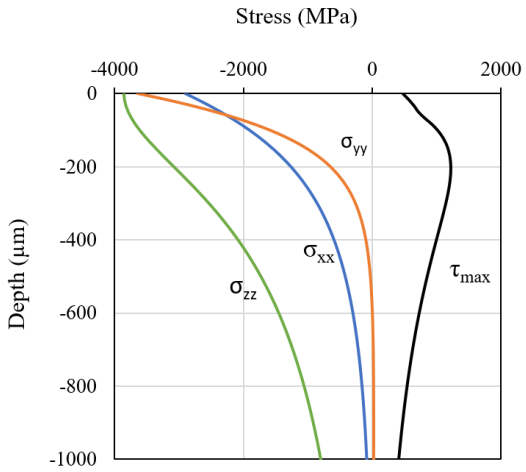

Figure 2 - Subsurface stress distribution under testing conditions (z: radial axis, y and x orthogonal axes)

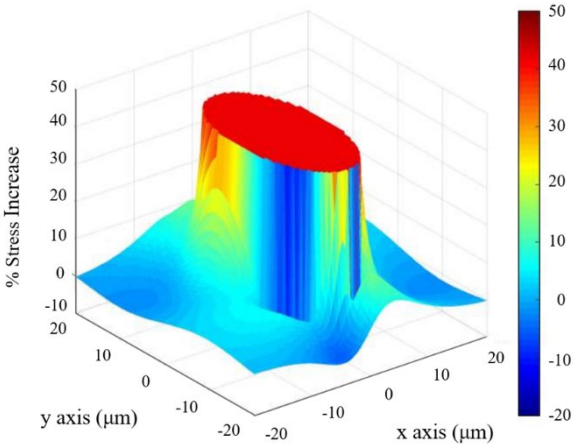

Figure 3 - Simulation of stress distribution around NMI in ball. Case 3 of the 12 failures investigated

shape, aspect ratio, position, and elastic modulus. The percent increment in stress is also reported.

The numerical stress simulation shows a stress gradient in the matrix volume surrounding the microinclusion related to a failure case (see Fig. 3 as an example).

The stress increment due to the microinclusions varies from 17% to 51% for the investigated failure cases.

In Fig. 4 a plot reports nominal (blue curve) subsurface equivalent stresses, calculated considering the contact force on a single ball due to the nominal experimental axial load (34400N). In the same plot, other curves are reported, representing the ideal stresses generated for increasing forces (Hertz load). The blue dots represent the nominal stress for each failed ball, in the point here the crack nucleated. Applying the Eshelby-Mura model, the stress increment due to the microinclusion experimentally found was evaluated (grey arrows). It can be observed that the presence of a microinclusion somehow "extends" the sub superficial volume where stresses become dangerous for crack nucleation in rolling contact fatigue.

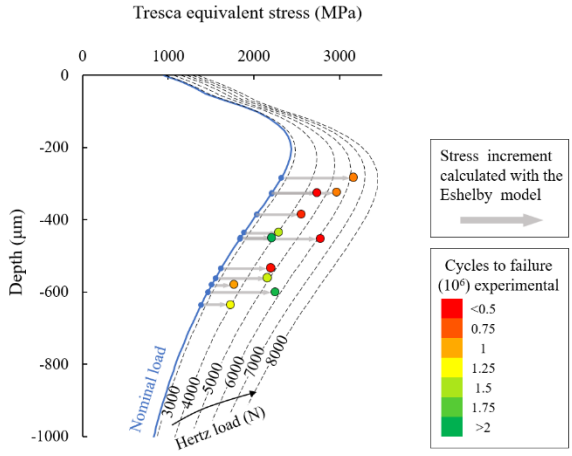

Figure 4 - Subsurface Tresca equivalent stresses calculated with and without microinclusions

This information stresses the critical importance of accounting quantitatively for all the parameters related to microinclusions (shape, dimension, aspect ratio, elastic modulus) and not only of its position for a correct

stress distribution calculation. Further information can be obtained from these results.

In Table 2 the calculated equivalent loads and L_{10} for failed balls are reported. L_{10} parameters are obtained according to Zaretsky model [19]. In rows, the different balls; N_L is the axial load applied to the bearing in the test rig during experimental testing; P_{eqn} is the nominal equivalent axial load, calculated according to catalogue indication for the estimation of the nominal L_{10} (i.e. 0.66 times the axial force acting on the bearing); T_L is the axial force that would produce in a homogeneous matrix the same Tresca stress that is due to the microinclusion, according to Eshelby; L_H is the Hertz load, i.e. the contact load applied to a single, homogeneous ball, generating at the microinclusion depth the same Tresca stress due to microinclusions; L_{10n} is the L_{10} nominal value calculated using the P_{eqn} value, i.e. without considering the effect of microinclusions; in the last column the cycles to failures N_f are reported. It can be observed that failures occurred for microinclusion positioned at depths for which the nominal stress is lower than the maximum nominal stress at the critical depth (2435 MPa @0,205 mm). for 5 over 12 specimens the calculated incremented stress is higher than the maximum nominal one. For the 7 other cases the incremented stress is in the range of 9 and 30% less than the maximum nominal stress at critical depth. The deepest microinclusion which caused failure occurred at 0,636 mm. The estimation of the incremented stress seems to be helpful in identifying a depth interval where microinclusion occur to be critical. This analysis can be extended to other parameters characterizing the microinclusion. A representative example is the shape: if the inclusion can be approximated as an elongated ellipse, the stress peak increment is greater.

This observation is supported by a wide range of inclusion types found in balls, with also different shapes and dimensions.

In [20] a further detailed analysis of the experimental results is reported.

In Figure 5 a failure surface including a microinclusion is reported

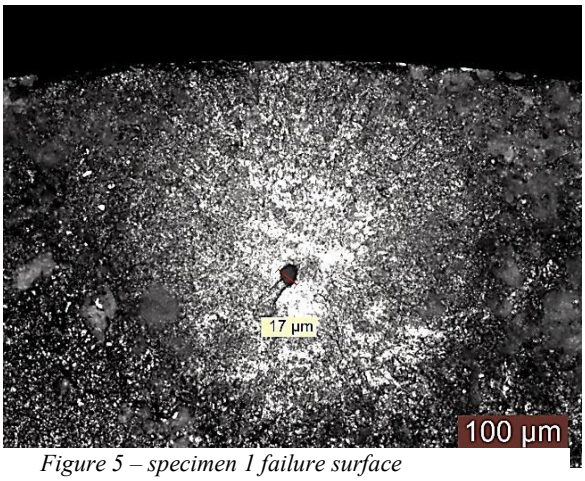

Figure 5 – specimen 1 failure surface

Table 1 - Microinclusions data and calculation results

ID	Composition	Dimension [µm]			Depth	Aspect ratio	σ_{nT}	σ_{iT}	σ_{inc}
		x	y	z	[µm]	xy	MPa	MPa	-
1	TiC (Ti carbide)	1.7	4.3	1.7	-453	0,40	1836	2776	51%
2	Al2O3 (Al oxyde)	1.7	2.7	1.7	-562	0,63	1550	2158	39%
3	Al2O3 (Al oxyde)	7.0	49.0	7.0	-600	0,14	1462	2245	54%
4	Al2O3 (Al oxyde)	12.5	12.5	12.5	-284	1,00	2320	3160	36%
5	TiC (Ti carbide)	4.5	4.5	4.5	-436	1,00	1886	2290	21%
6	Al2O3 (Al oxyde)	12.3	10.0	10.0	-326	0,81	2210	2969	34%
7	Al2O3 (Al oxyde)	3.5	2.0	2.0	-450	0,57	1846	2206	20%
8	Al2O3 (Al oxyde)	2.5	0.5	0.5	-636	0,20	1384	1728	25%
9	Al2O3 (AL oxyde)	4.0	1.0	1.0	-386	0,25	2034	2552	25%
10	CaO (Ca Oxide)	4.0	2.0	2.0	-580	0,50	1508	1768	17%
11	Al2O3 (Al oxyde)	7.5	7.5	7.5	-535	1,00	1616	2200	36%
12	Si+Al+Ca	15.0	15.0	5.0	-327	1,00	2208	2737	24%

Table 2 – Calculated equivalent loads for failed balls

ID	N_L [N]	P_{eqn} [N]	T_L [N]	L_H [N]	L_{10n} (10^6 cycles)	N_f (10^6 cycles)
1	34400	22704	74445	6100	1.51	0.46
2	34400	22704	59800	4900	1.51	1.4
3	34400	22704	39053	3200	1.51	1.94
4	34400	22704	75666	6200	1.51	0.87
5	34400	22704	48817	4000	1.51	1.45
6	34400	22704	67123	5500	1.51	0.46
7	34400	22704	47596	3900	1.51	3.75
8	34400	22704	48817	4000	1.51	1.28
9	34400	22704	53698	4400	1.51	0.61
10	34400	22704	45155	3700	1.51	0.97
11	34400	22704	58580	4800	1.51	0.54
12	34400	22704	54919	4500	1.51	0.87

4. Conclusions

The target of the activity was to evaluate the influence of microinclusions on the fatigue life of rolling balls, accounting for shape, dimension, aspect ratio, location, and Young's modulus of microinclusions. For this reason, the effect on the stress field of balls made of 100Cr6 was investigated.

Many sets of balls were tested in bearings thanks to a dedicated test rig. Furthermore, the fracture analyses were assessed thanks to a gauge meter, an optical microscope, and a Scanning Electron Microscope.

A numerical solver that implements the Eshelby solution for the inclusion problem was developed to analyze the cases above. Some simulations were made to understand the functionalities of the code and the effect of the different parameters: dimension, shape, depth, chemical composition, and configuration were evaluated. Moreover, the code was useful to simulate the stress state of the experimental cases.

Twelve failed balls were considered, for each case all the inclusion properties were found and the stress state around microinclusion was evaluated.

The survey pointed out that inclusions that are shallower than a certain value are not critical for failures, according to [13], and at the same time, no inclusions close to the surface were found, according to the Hertz theory. These aspects suggest that there is a defined depth range for which the inclusion, together with its own properties, is critical.

Further discussion and further development of this approach can follow, considering that the elastic modulus of the matrix changes during damaging processes, according to [3], and thus the estimation of Tresca stress by means of Eshelby model should take into account of this evolving phenomenon or, according to [3], couple the stress fields due to microinclusion and to Hertzian contact. Also, the interaction between microinclusions can be modelled in a more detailed way, above all in the case they have different compositions.

Nomenclature

σ_{nT} *equivalent Tresca stress at microinclusion location*

σ_{iT} *equivalent Tresca stress at microinclusion boundary according to Eshelby model*

σ_{inc} increment of stress from nominal stress without inclusion and with inclusion)

P_{eqn} nominal equivalent axial load, calculated according to catalogue indication

L_{10} catalogue indication of life in millions of cycles

L_{10n} life in millions of cycles calculated using the P_{eqn} value, i.e. without considering the effect of microinclusions

L_H Hertz load, i.e. the contact load applied to a single, homogeneous ball, generating at the microinclusion depth the same Tresca stress due to microinclusions

N_L axial load applied to the bearing in the test rig during experimental testing

N_f cycles to failures

T_L axial force that would produce in a homogeneous matrix the same Tresca stress that is due to the microinclusion

References

Example:

[1] J. Halme and P. Andersson, “Rolling contact fatigue and wear fundamentals for rolling bearing diagnostics - State of the art,” Proc. Inst. Mech. Eng. Part J J. Eng. Tribol., 2010, doi: 10.1243/13506501JET656.

[2] N. K. Arakere, “Gigacycle rolling contact fatigue of bearing steels: A review,” Int. J. Fatigue, vol. 93, pp. 238–249, Dec. 2016, doi: 10.1016/j.ijfatigue.2016.06.034.

[3] T. Beyer, F. Sadeghi, T. Chaise, J. Leroux, and D. Nelias, “A coupled damage model and a semi-analytical contact solver to simulate butterfly wing formation around non-metallic inclusions,” Int. J. Fatigue, 2019, doi: 10.1016/j.ijfatigue.2019.05.029.

[4] N. Tsunekage, K. Hashimoto, T. Fujimatsu, and K. Hiraoka, “Initiation behavior of crack originated from non-metallic inclusion in rolling contact fatigue,” J. ASTM Int., 2010, doi: 10.1520/JAI102612.

[5] Y. Unigame, K. Hiraoka, I. Takasu, and Y. Kato, “Evaluation Procedures of Nonmetallic Inclusions in Steel for Highly Reliable Bearings,” in Bearing Steel Technology-Advances and State of the Art in Bearing Steel Quality Assurance: 7th Volume, 100 Barr Harbor Drive, PO Box C700, West Conshohocken, PA 19428-2959: ASTM International, 2009, pp. 34-34–8.

[6] F. J. Ebert, “Fundamentals of Design and Technology of Rolling Element Bearings,” Chinese J. Aeronaut., 2010, doi: 10.1016/S1000-9361(09)60196-5.

[7] H. Fu et al., “The relationship between 100Cr6 steelmaking, inclusion microstructure and rolling contact fatigue performance,” Int. J. Fatigue, 2019, doi: 10.1016/j.ijfatigue.2018.11.011.

[8] T. Makino et al., “Effect of defect shape on rolling contact fatigue crack initiation and propagation in high strength steel,” Int. J. Fatigue, vol. 92, pp. 507–516, Nov. 2016, doi: 10.1016/j.ijfatigue.2016.02.015.

[9] K. Hashimoto, T. Fujimatsu, N. Tsunekage, K. Hiraoka, K. Kida, and E. C. Santos, “Study of rolling contact fatigue of bearing steels in relation to various oxide inclusions,” Mater. Des., vol. 32, no. 3, pp. 1605–1611, Mar. 2011, doi: 10.1016/j.matdes.2010.08.052.

[10] Y. Murakami and N. Yokoyama, “Influence of Hydrogen Trapped by Inclusions on Fatigue Strength of Bearing Steel,” in Bearing Steel Technology, 100 Barr Harbor Drive, PO Box C700, West Conshohocken, PA 19428-2959: ASTM International, 2009, pp. 113-113–12.

[11] J. Lai, T. Lund, K. Rydén, A. Gabelli, and I. Strandell, “The fatigue limit of bearing steels - Part I: A pragmatic approach to predict very high cycle fatigue strength,” Int. J. Fatigue, 2012, doi: 10.1016/j.ijfatigue.2011.09.015.

[12] S. M. Moghaddam et al., “Effect of non-metallic inclusions on butterfly wing initiation, crack formation, and spall geometry in bearing steels,” Int. J. Fatigue, vol. 80, pp. 203–215, Nov. 2015, doi: 10.1016/j.ijfatigue.2015.05.010.

[13] A. Gabelli, J. Lai, T. Lund, K. Rydén, I. Strandell, and G. E. Morales-Espejel, “The fatigue limit of bearing steels – Part II: Characterization for life rating standards,” Int. J. Fatigue, vol. 38, pp. 169–180, May 2012, doi: 10.1016/j.ijfatigue.2011.12.006.

[14] J. Courbon, G. Lormand, G. Dudragne, P. Daguier, and A. Vincent, “Influence of inclusion pairs, clusters and stringers on the lower bound of the endurance limit of bearing steels,” Tribol. Int., 2003, doi: 10.1016/S0301-679X(03)00076-8.

[15] M. Oezel, T. Janitzky, P. Beiss, and C. Broeckmann, “Influence of steel cleanliness and heat treatment conditions on rolling contact fatigue of 100Cr6,” Wear, 2019, doi: 10.1016/j.wear.2019.04.026.

[16] J.D. Eshelby, “The determination of the elastic field of an ellipsoidal inclusion, and related problems”, Proceedings of the Royal Society A, pp. 376-396, 1957, https://doi.org/10.1098/rspa.1957.0133

[17] ASTM, “E45-18a Standard Test Methods for Determining the Inclusion Content of Steel,” ASTM Int. Conshohocken, PA, www.astm.org, 2018, doi: 10.1520/E0045-18A.

[18] “Mechanical Behavior of Materials“, Global Edition, V edition, N.E. Dowling et al, Pearson Ed. 2019.

[19] E. V Zaretsky, “Rolling bearing life prediction, theory, and application,” NASA Tech. Reports, 2013.

[20] R. Sesana, E. Ossola, S. Pagliassotto, S. Rizzo, E. Brusa, “Influence of microinclusion in life of rolling elements: Experimental, microstructural, analytical and numerical investigation”, International Journal of Fatigue 139 (2020) 1057.